ChemComm

Energy-resolved distribution of electron traps for O/S-doped carbon nitrides by reversed double-beam photoacoustic spectroscopy and the photocatalytic reduction of Cr(VI)

Journal:	*ChemComm*
Manuscript ID	CC-COM-12-2019-009988.R1
Article Type:	Communication

COMMUNICATION

Energy-resolved distribution of electron traps for O/S-doped carbon nitrides by reversed double-beam photoacoustic spectroscopy and the photocatalytic reduction of Cr(VI)

Received 00th January 20xx,
Accepted 00th January 20xx

DOI: 10.1039/x0xx00000x

Chitiphon Chuaicham[a], Sekar Karthikeyan[a], Radheshyam Pawar[a], Yihuang Xiong[b], Ismaila Dabo[b], Bunsho Ohtani[c], Yoonyoung Kim[d,e], Jun Tae Song[d,e], Tatsumi Ishihara[d,e] and Keiko Sasaki[a,c*]

We report on the first time the identification of heteroatom-doped and undoped C_3N_4 with the energy-resolved distribution of electron traps (ERDT) near the conduction band bottom position (CBB) using reversed double-beam photoacoustic spectroscopy. The ERDT/CBB pattern are used to classify the type of elemental doping in C_3N_4, related to photocatalytic efficiency.

Identification, with detailed determination structures and developed material nomenclature, are the areas most focused on in the versatile research field to understand the hidden possessions in material science. One of the most common analysing techniques used to examine the bulk properties of the solid materials, X-ray diffraction (XRD), designates the crystalline and amorphous phases and elemental compositions in developed materials. Fourier-transform infrared spectroscopy (FTIR) is a technique used to obtain an infrared spectrum of absorption or emission of solid materials that provide information about functional groups and covalent bonds present in the materials. The Brunauer–Emmett–Teller (BET) theory aims to explain the physical adsorption of gas molecules on a solid surface and serves as the basis for measuring specific surface area particle sizes and may provide some information about the structural or textural properties of the developed materials. However, in versatile material applications, the surface properties of advanced materials have a significant influence on the activities and efficacy of the concerned area of the applications. Especially in photocatalysis, surface electronic properties, such as the charge transfer and electronic properties through the surfaces of solid materials, are essential in understanding specific photocatalytic mechanisms. Hence, it is necessary to identify the surface electronic properties in the solid photocatalyst using electrochemical techniques.

Recently, Ohtani et al. have developed a novel analytical method, reversed double-beam photoacoustic spectroscopy (RDB-PAS), for measuring the energy-resolved distribution of electron traps (ERDT). The principles and detailed information regarding advanced RDB-PAS techniques are narrated in previous reports.[1] The RDB-PAS technique successfully identified the surface properties of many photocatalysts and most of the metal-oxide powder samples in the study.[1-3] Fingerprint ERDTs combined with conduction band bottom position (CBB) patterns may be useful in the correct identification of respective solids surfaces (electronic properties).

In this study, undoped C_3N_4, O-doped C_3N_4, and S-doped C_3N_4 were synthesized using diverse precursors for the photocatalytic reduction of Cr(VI) to Cr(III) under visible light irradiation. The guest elements of O/S in the precursors (**Fig. S1**) can be doped into the C_3N_4 structure during synthesis. The obtained products from melamine, dicyandiamide, urea, cyanuric acid, thiourea, and ammonium thiocyanate as precursors were denoted as CMA, CDM, CU, CCA, CT, and CAT, respectively. Moreover, the calcination of melamine in the N_2 flow also was prepared and denoted as CMN. In the primary stages of the research, we observed that the typical XRD and FTIR methods were not sufficient to identify the type of heteroatom doping in the main electronic structure of C_3N_4. Similarly, the optical property results could not be used to identify the original and heteroatom-doped C_3N_4. Therefore, we are reporting on the identification of surface and bulk electronic properties using the RDB-PAS technique to generate ERDT patterns as a fingerprint of different doping elements in the C_3N_4 structure.

[a] *Department of Earth Resources Engineering, Faculty of Engineering, Kyushu University, 744 Motooka, Nishiku, Fukuoka 819-0395, Japan, E-mail: keikos@mine.kyushu-u.ac.jp*
[b] *Department of Materials Science and Engineering, The Pennsylvania State University, University Park, Pennsylvania 16802, United States*
[c] *Institute for Catalysis, Hokkaido University, Sapporo 001-0021, Japan.*
[d] *Department of Applied Chemistry, Faculty of Engineering, Kyushu University, 744 Motooka, Nishiku, Fukuoka 819-0395, Japan*
[e] *International Institute for Carbon-Neutral Energy Research (I2CNER), 744 Motooka, Nishiku, Fukuoka 819-0395, Japan*
† Footnotes relating to the title and/or authors should appear here.
Electronic Supplementary Information (ESI) available: [details of any supplementary information available should be included here]. See DOI: 10.1039/x0xx00000x

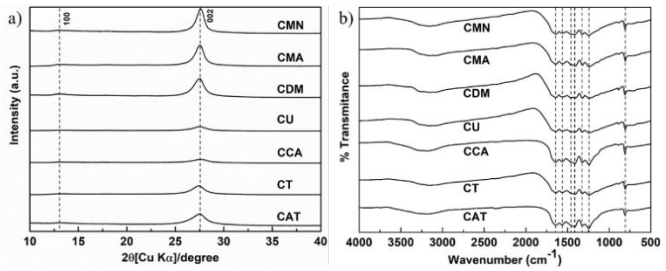

Fig. 1 a) PXRD patterns and b) FTIR spectra of different heteroatom-doped C_3N_4.

XRD patterns of synthesized undoped C_3N_4 (CMN, CMA, and CDM), O-doped C_3N_4 (CU and CCA), and S-doped C_3N_4 (CT and CAT) photocatalysts from diverse precursors were presented in **Fig. 1a**. The predominant diffraction peaks of all synthesized catalysts can be observed at 2θ around 12.9° with a 100 plan, corresponding to the interlayer stacking distance of aromatic units with d = 0.326 nm. The main diffraction peak of the 002 plan shown at 2θ about 27.6° corresponded to an in-plane structural distance of C_3N_4 (d=0.681 nm).[4] The heteroatom doped C_3N_4 (CU, CCA, CT, and CAT) displayed a lower intensity and broader diffraction peaks of the 002 plan than those of the undoped C_3N_4 (CMN, CMA, and CDM), indicating that the O or S-containing precursors affected the crystallization and polymerization of C_3N_4 due to its strong C-O or C-S bonding, leading to defects in the final product.[5] However, no obvious 2θ differences were detected amongst the family of doped C_3N_4, suggesting that these contain a similar in-plane structural recapping motif and void-to-void distance (d =0.681 nm).[6] This distance due to the collapse structure of the tris-s-triazine unit was only slightly lower than the void-to-void distance (0.73 nm). For example, indexed 2θ peaks at 13.1° and 27.3°.[6] Furthermore, the FTIR spectra of C_3N_4 synthesized using the different precursors were presented in **Fig. 1b**. All of sample showed similar spectra even if it has O/S in the main structure **(EIS)**. Elemental compositions of C_3N_4 with and without heteroatom doping were summarized in **Table S1**. Around 2–3 wt% of O and 0.5–0.1 wt% of S were included in O-doped and S-doped C_3N_4, respectively.

The surface composition of undoped C_3N_4 and heteroatom-doped C_3N_4 was investigated by XPS. As shown in **Fig. S2a**, the N 1s spectra of all samples were deconvoluted into four peaks at 398.5 eV, 399.8 eV, 402.4 eV, and 405.9 eV, corresponding to the sp^2 aromatic nitrogen bonded to carbon (C=N-C), tertiary nitrogen groups $N(-C)_3$, quaternary N in the aromatic cycles, and π excitations, respectively. The O 1s spectra (**Fig. S2b**) of undoped C_3N_4 and O-doped C_3N_4 were observed and separated into two peaks to confirm the presence of O in the synthetic samples. The peak around 532 eV is ascribed to C=O, while the peak cantered at 534 eV can be attributed to surface adsorbed water. In comparison to the O content in the structure of C_3N_4, XPS surface sensitivity was calculated using N 1s and the peak area of C=O. The O-doped C_3N_4 clearly exhibits a higher O/N ratio than that of the undoped C_3N_4, indicating that O-doped C_3N_4 can be synthesized using urea and cyanuric acid (**Table S2**). However, signals of the S 2p orbital in the S-doped C_3N_4 cannot be observed due to low S content in the samples.

The specific surface area (SSA) of the samples was obtained from N_2 adsorption-desorption measurements. The adsorption-desorption isotherms and SSAs of all samples are shown in **Fig. S3** and **Table S3**, respectively. The O-doped C_3N_4 samples exhibited higher SSAs than the undoped C_3N_4, and S-doped C_3N_4, indicating that the destruction of the C_3N_4 skeleton occurred after O is doped in the main structure.[7]

The optical properties of undoped C_3N_4 and heteroatom doped C_3N_4 were examined by an ultraviolet–visible light (UV–vis) diffuse reflectance spectroscopy (DRS) as displayed in **Fig. S4a**. All the photocatalysts exhibited high visible light absorption from 400 nm to 550 nm, indicating that the synthesized samples can be utilized as potential photocatalysts in the visible light region. In addition, the calculated energy bandgap (*Eg*) of all samples was calculated as presented in **Fig. S4b**. The *Eg* of CMN, CMA, CDM, CU, CCA, CT, and CAT were estimated to be 2.77 eV, 2.74 eV, 2.76 eV, 2.88 eV, 2.92 eV, 2.72 eV, and 2.71 eV, respectively. Compared with CMN, CMA, and CDM (undoped C_3N_4), CT and CAT (S-doped C_3N_4) displayed a lower *Eg*, while CU and CCA (O-doped C_3N_4) showed a higher *Eg* compared with undoped C_3N_4. This is a similar trend to previous reports.[5, 7-9] The redshift of the absorption spectra to the more visible light region and decreasing E*g* of CT and CAT enhance the light absorption in the visible light region, resulting in the generation of more electron and hole pairs which can improve the photocatalytic activity of the samples. In contrast, CU and CCA, which have low crystallinity and a thin-layer of C_3N_4, show a blue shift in absorption spectra and a larger E*g* than that of the undoped C_3N_4, which results from the quantum confinement effect.[7, 10] The recombination of photogenerated electron-hole pairs of all photocatalysts was examined by photoluminescence spectroscopy. **In Fig. S5**, the undoped C_3N_4 (CMN, CMA, and CDM) showed a higher photoluminescence intensity than that of O-doped C_3N_4 (CU and CCA) and S-doped C_3N_4 (CT and CAT), indicating that the heteroatom doping in the C_3N_4 structure can avoid electron and hole recombination.

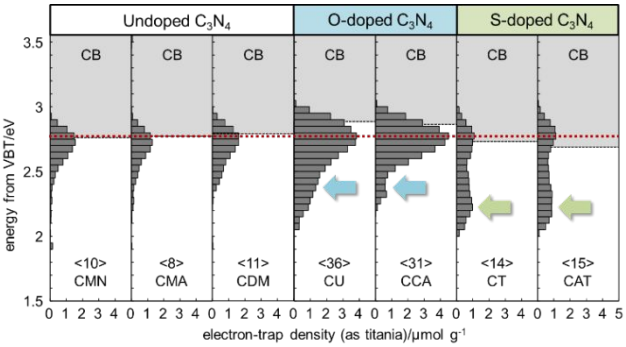

Fig. 2 ERDT patterns with CBB position of heteroatom-doped and undoped C_3N_4 photocatalysts. The number in < > denotes the total density of ETs in the unit of μmol g^{-1}.

Based on the XRD, FTIR, and DRS results, it is difficult to classify the type of doping elements in C_3N_4, related to photocatalytic activity. Thus, the newly developed characterization technique, RDB-PAS, was applied to study not only the surface structure but also the bulk electronic structure of photocatalysts.[1, 2] This study is the first instance of applying the RDB-PAS to the metal-

free photocatalyst C_3N_4. ERDT patterns of all samples provided information about electron accumulation in the electron traps (ETs) near the CBB, which expressed the ETs levels in the samples. Surprisingly, the C_3N_4 from the different precursors, even if they have similar XRD patterns and FTIR spectra, resulted in differently shaped ERDT patterns and total densities of ETs as shown in **Fig. 2**. All, the family of undoped C_3N_4 (CMN, CMA, and CDM), O-doped C_3N_4 (CU and CCA), S-doped C_3N_4 (CT and CAT) displayed similar levels of accumulated electrons in the ETs around 2.7 eV near the CBB, which may be a characteristic of C_3N_4. However, the heteroatom-doped C_3N_4 (CU, CCA, CT, and CAT) resulted in different shapes of ERDT patterns from the undoped C_3N_4. The O-doped C_3N_4 (CU and CCA) presented higher electron accumulation levels in the ETs around 2.7 eV than that of the undoped C_3N_4, leading to an increase in total electron density in ETs. In addition, the new ETs around 2.2 eV, which were created by the O/S impurities in the C_3N_4 structure, can be detected in the O-doped C_3N_4 and clearly observed in the S-doped C_3N_4. The changing ERDT pattern, total ET density, and CBB level after doping with O/S in C_3N_4 can be used to identify the type of doping elements. To examine the similarities of synthesized C_3N_4 based on different heteroatom dopings using different precursors, the overall degrees of coincidence (ζ) of every pair of sample comparisons were calculated based on three factors: ERDT-pattern shape (ζ(a)), total electron-trap density (ζ(b)), and CBB position (ζ(c)).[1] The ζ(c) reflected the property of the bulk structure while the ζ(a) and ζ(b) contribute to the surface structure property information on the "identicalness" or "similarity" without arbitrariness. The ζ of the photocatalyst can be evaluated using the following equation:

$$\zeta = \zeta(a) * \zeta(b)^{\bar{2}} * \zeta(c)^2. \quad (1)$$

Table 1 Degrees of coincidence ζ summary for different heteroatom-doped and undoped C_3N_4 photocatalysts

		CMN	CMA	CDM	CU	CCA	CT	CAT
CMN	ζ(a)		0.88	0.79	0.50	0.68	0.14	0.11
	ζ(b)		0.80	0.91	0.28	0.32	0.71	0.67
	ζ(c)		0.99	1.00	0.96	0.95	0.98	0.98
	ζ		0.77	0.75	0.25	0.37	0.12	0.09
CMA	ζ(a)	0.88		0.80	0.61	0.66	0.24	0.21
	ζ(b)	0.80		0.73	0.22	0.32	0.71	0.67
	ζ(c)	0.99		0.99	0.95	0.94	0.99	0.99
	ζ	0.77		0.68	0.27	0.35	0.20	0.17
CDM	ζ(a)	0.79	0.80		0.64	0.76	0.22	0.22
	ζ(b)	0.91	0.73		0.31	0.35	0.79	0.73
	ζ(c)	1.00	0.99		0.96	0.95	0.99	0.98
	ζ	0.75	0.68		0.34	0.43	0.20	0.19
CU	ζ(a)	0.50	0.61	0.64		0.70	0.59	0.60
	ζ(b)	0.28	0.22	0.31		0.86	0.39	0.42
	ζ(c)	0.96	0.95	0.96		0.99	0.94	0.94
	ζ	0.25	0.27	0.34		0.64	0.35	0.37
CCA	ζ(a)	0.68	0.66	0.76	0.70		0.47	0.49
	ζ(b)	0.32	0.32	0.35	0.86		0.45	0.48
	ζ(c)	0.95	0.94	0.95	0.99		0.93	0.93
	ζ	0.37	0.35	0.43	0.64		0.29	0.31
CT	ζ(a)	0.14	0.24	0.22	0.59	0.47		0.88
	ζ(b)	0.71	0.71	0.79	0.39	0.45		0.93
	ζ(c)	0.98	0.99	0.99	0.94	0.93		1.00
	ζ	0.12	0.20	0.20	0.35	0.29		0.85
CAT	ζ(a)	0.11	0.21	0.22	0.60	0.49	0.88	
	ζ(b)	0.67	0.67	0.73	0.42	0.48	0.93	
	ζ(c)	0.98	0.99	0.98	0.94	0.93	1.00	
	ζ	0.09	0.17	0.19	0.37	0.31	0.85	

Table 1 shows the ζ for each sample pair. In comparison with CMN, the highest overall degree of coincidence values (ζ) are given by CMA and CDM due to their high values of ζ(a) and ζ(b), which confirms the similarity of undoped C_3N_4. Moreover, the comparison between CU and CCA shows a high ζ value, while the comparison of CT and CAT also provides a high ζ value. Based on the ζ, the synthetic C_3N_4 samples from diverse precursors can be classified into three groups, undoped C_3N_4 (CMN, CMA, and CDM), O-doped C_3N_4 (CU and CCA), and S-doped C_3N_4 (CT and CAT), due to the ζ of each group samples being higher than 0.6, which suggests a high level of similarity for a pair samples. Thus, the combination of ERDT and CBB (ERDT/CBB pattern) can be used as a fingerprint to identify the doping type of C_3N_4.

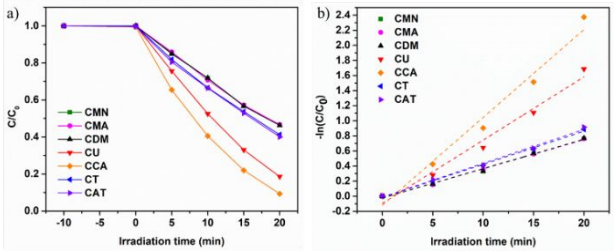

Fig. 3 (a) Photocatalytic reduction of Cr(VI) and (b) kinetics plots for the heteroatom-doped and undoped C_3N_4 photocatalysts at different time intervals

Furthermore, a photocatalytic reduction of $Cr_2O_7^{2-}$ was performed to understand the effects of doping elements related to the ERDT/CBB pattern as showed **Figs. 3a and b**. The S doped C_3N_4 (CT and CAT) showed a higher photocatalytic efficiency than that of the undoped C_3N_4 (CMN, CMA, and CDM), while the photocatalytic activity and rate constants dramatically increased in the O-doped C_3N_4 (CU and CCA). The improvement in Cr(VI) reduction efficiency by O/S-doped C_3N_4 may be a reason for the enhancement of light absorption abilities, improved separation of photogenerated charge carriers, and an increase in SSAs[11-13], in relation to increase in ζ(b). Moreover, the degree of coincidence for a photocatalytic reduction in Cr(VI) (ζ_{PC}) for each sample pair was calculated to elucidate the relationship between ERDT/CBB patterns and the photocatalytic Cr(VI) reduction (**Table S4**). The high ζ_{PC} (> 0.9) for CU and CCA can be observed along with a high value of ζ (> 0.6), while the low value of ζ provides a low ζ_{PC}, indicating that the ζ of ERDT/CBB pattern induces ζ_{PC}. In comparison, each sample group (undoped C_3N_4, O-doped C_3N_4 and S-doped C_3N_4) with high ζ showed high similarity of photocatalytic Cr(VI) reduction efficiency. Thus, the photocatalytic activity of undoped and doped C_3N_4 could be predicted by checking ζ of ERDT/CBB pattern. If sample pairs showed ζ ≥ 0.6, it might have identical photocatalytic performances of sample pairs (ζ_{PC} ≥ 0.9). The ERDT/CBB patterns forming the RDB-PAS technique can be used not only to identify the different types of heteroatom doping in C_3N_4 (instead of using the traditional techniques: XRD and FTIR) but also to predict photocatalytic performance. For the reduction mechanism of Cr(VI), with visible-light illumination, C_3N_4 produces photogenerated electron-hole pairs by absorbing the photon energy.[14] The photogenerated electrons can be easily transferred to the C_3N_4 surface and accumulated in new donor levels near the CBB interface; subsequently, the excited electron can reduce the $Cr_2O_7^{2-}$ to Cr^{3+} on the C_3N_4 surface. The suppression of electron-hole pair recombination and charge transfer by heteroatom

doped C_3N_4 which confirmed by PL, EIS and TRPL (**Fig. S6a,b, Table S5),** show the improvement of photocatalytic Cr(VI) reduction activity.

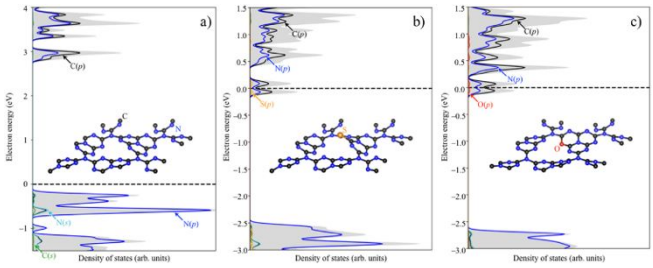

Fig. 4 Projected state densities of (a) C_3N_4, (b) S-doped C_3N_4, and (c) O-doped C_3N_4. Doping of S and O in C_3N_4 cause the formation of mid-gap states that are close to the conduction band.

To confirm the location of S and O in the C_3N_4 structure and the electronic states generated by guest elements, electronic-structure calculations are performed at the Perdew-Burke-Ernzerhof (PBE) semi-local level of density-functional theory[15] using the projected augmented wave method implemented in the Vienna Ab-initio Simulation Package (VASP).[16] The substitution of nitrogen at three different S and O positions in the C_3N_4, center, edge, and connection, are denoted as N_{center}, N_{edge}, and $N_{connect}$, respectively, and are shown in **Fig. S7**. The substitution energy of S (ΔE_S) at N_{center}, N_{edge}, and $N_{connect}$ are calculated to be 2.20 eV, 0.92 eV, and 1.84 eV, respectively, indicating that N_{edge} is the preferential doping site for S. Similarly, oxygen substitution is favored at N_{edge}, with substitution energy O (ΔE_O) of –0.32 eV, –1.15 eV, and 0.32 eV at the N_{center}, N_{edge}, and $N_{connect}$ sites, respectively. We thus adopt N_{edge} substitution as the relevant doping geometry for subsequent projected density of states (PODS) calculations as shown in **Fig. 4**. It is clear that the valence band (VB) and conduction band (CB) of undoped C_3N_4 (CMN, CMA, and CDM), O-doped C_3N_4 (CU and CCA), and S-doped C_3N_4 (CT and CAT) are dominated by the p orbital of N and C. Importantly, the substitutional doping of S and O induces mid-gap states that are close to the CB, as shown in **Figs. 4b-c**. These results confirm the generation of intermediate electronic levels after doping S and O into C_3N_4 structures, which correspond to the observation of ETs levels in the ERDT/CBB patterns of the heteroatom-doped C_3N_4 samples.

In summary, this work provides a new method to characterize and classify C_3N_4 both with and without heteroatom doping using RDB-PAS. The ERDT patterns, which are obtained by RDB-PAS, along with the CBB, were significantly influenced by doped atoms but not affected by the precursors of C_3N_4. The different heteroatom-doped C_3N_4 showed different ERDT/CBB pattern shapes, which can be used to identify the similarities or differences in the family of C_3N_4 photocatalysts. The sample in each group of undoped C_3N_4 (CMN, CMA, and CDM), O-doped C_3N_4 (CU and CCA), and S-doped C_3N_4 (CT and CAT) exhibited similar ζ values which are calculated from the ERDT/CBB patterns, confirming that the similar doping elements of C_3N_4 might show similar ERDT/CBB pattern shapes and ζ(b). Moreover, the photocatalytic Cr(VI) reduction performances of differently doped C_3N_4 samples are related to their ERDT/CBB patterns. Thus, the ERDT/CBB analysis can be used as an alternative method to identify the different doping element in C_3N_4 and their photocatalytic efficiency.

This work was supported by the Japan Society for the Promotion of Science (JSPS) KAKENHI Grant Number JP19H00883 and JP18F18387, Cooperative Research Programs at Hokkaido University Institute for Catalysis (Nos. 18A1001 and 19B1002) and “Progress 100” (World Premium International Researcher Invitation Program) in Kyushu University through operating expense grants of the Ministry of Education, Culture, Sports, Science and Technology. ID and YX acknowledge financial support from the National Science Foundation under Grant No. DMREF- 1729338. A part of this work was conducted in Kyushu University, supported by Nanotechnology Platform Program (Molecule and Material Synthesis) of the Ministry of Education, Culture, Sports, Science and Technology (MEXT), Japan.

Conflicts of interest

The authors declare that there is no conflict of interest.

Notes and references

1. A. Nitta, M. Takase, M. Takashima, N. Murakami and B. Ohtani, *Chem Commun (Camb)*, 2016, **52**, 12096-12099.
2. A. Nitta, M. Takashima, N. Murakami, M. Takase and B. Ohtani, *Electrochimica Acta*, 2018, **264**, 83-90.
3. P. Ketwong, M. Takashima, A. Nitta, P. Pookmanee and B. Ohtani, *Journal of Environmental Chemical Engineering*, 2018, **6**, 2048-2054.
4. X. Wang, K. Maeda, A. Thomas, K. Takanabe, G. Xin, J. M. Carlsson, K. Domen and M. Antonietti, *Nat Mater*, 2009, **8**, 76-80.
5. M. Ismael, Y. Wu, D. H. Taffa, P. Bottke and M. Wark, *New Journal of Chemistry*, 2019, **43**, 6909-6920.
6. A. Thomas, A. Fischer, F. Goettmann, M. Antonietti, J. O. Muller, R. Schlogl and J. M. Carlsson, *Journal of Materials Chemistry*, 2008, **18**, 4893-4908.
7. Y. Wang, L. Rao, P. Wang, Y. Guo, X. Guo and L. Zhang, *Environmental science and pollution research international*, 2019, **26**, 15710-15723.
8. K. Wang, Q. Li, B. S. Liu, B. Cheng, W. K. Ho and J. G. Yu, *Appl Catal B-Environ*, 2015, **176**, 44-52.
9. Y. Luo, J. Wang, S. Yu, Y. Cao, K. Ma, Y. Pu, W. Zou, C. Tang, F. Gao and L. Dong, *Journal of Materials Research*, 2018, **33**, 1268-1278.
10. X. Zhang, X. Xie, H. Wang, J. Zhang, B. Pan and Y. Xie, *J Am Chem Soc*, 2013, **135**, 18-21.
11. R. Tang, R. Ding and X. Xie, *Water science and technology : a journal of the International Association on Water Pollution Research*, 2018, **78**, 1023-1033.
12. J. Li, B. Shen, Z. Hong, B. Lin, B. Gao and Y. Chen, *Chem Commun (Camb)*, 2012, **48**, 12017-12019.
13. G. Mamba and A. K. Mishra, *Appl Catal B-Environ*, 2016, **198**, 347-377.
14. A. Ali, X. D. Li, J. L. Q. Song, S. Y. Yang, W. T. Zhang, Z. M. Zhang, R. X. Xia, L. X. Zhu and X. L. Xu, *J Phys Chem C*, 2017, **121**, 21096-21104.
15. J. P. Perdew, K. Burke and M. Ernzerhof, *Phys Rev Lett*, 1996, **77**, 3865-3868.
16. G. Kresse and J. Furthmuller, *Physical review. B, Condensed matter*, 1996, **54**, 11169-11186.

Table of contents

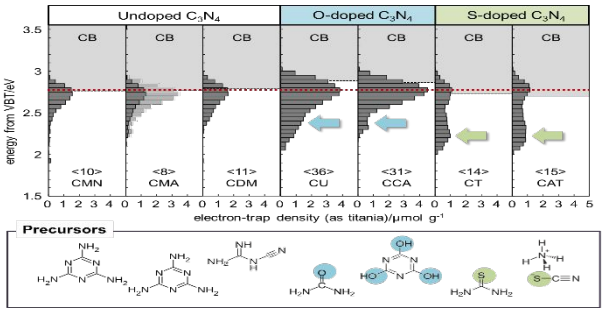

ERDT patterns with CBB position of undoped and O/S-doped C_3N_4